Front. Energy 2022, 16(3): 460–470
https://doi.org/10.1007/s11708-022-0825-9

RESEARCH ARTICLE

Chuanke LIU, Zhizhu HE

High heat flux thermal management through liquid metal driven with electromagnetic induction pump

Abstract In this paper, a novel liquid metal-based minichannel heat dissipation method was developed for cooling electric devices with high heat flux. A high-performance electromagnetic induction pump driven by rotating permanent magnets is designed to achieve a pressure head of 160 kPa and a flow rate of 3.24 L/min, which could enable the liquid metal to remove the waste heat quickly. The liquid metal-based minichannel thermal management system was established and tested experimentally to investigate the pumping capacity and cooling performance. The results show that the liquid metal cooling system can dissipate heat flux up to 242 W/cm^2 with keeping the temperature rise of the heat source below 50°C. It could remarkably enhance the cooling performance by increasing the rotating speed of permanent magnets. Moreover, thermal contact resistance has a critical importance for the heat dissipation capacity. The liquid metal thermal grease is introduced to efficiently reduce the thermal contact resistance (a decrease of about 7.77 × 10^{-3} °C/W). This paper provides a powerful cooling strategy for thermal management of electric devices with large heat power and high heat flux.

Keywords high heat flux, liquid metal, electromagnetic pump, minichannel heat sink, thermal interface material

1 Introduction

As electronic devices develop rapidly toward high-power densities and miniaturization, waste heat as inevitable byproducts has a significant influence on the electronic apparatus and even induces malfunctioning and degradation of electronics [1]. Many high-efficient cooling technologies have been developed for cooling compact light-emitting diodes (LEDs) [2], computer chips [3], lithium-ion batteries [4], and insulated gate bipolar transistors (IGBTs) [5]. It is a significant challenge to develop an effective thermal management method for high power devices in a limited space [6,7]. Recently, the micro/mini-channel-based cooling technology proposed by Tuckerman and Pease [8] has been extensively studied for large power heat removal [9,10]. The reason for this is that micro/mini-channel-based heat sinks have an excellent heat transfer coefficient and large convective heat transfer area. Consequently, micro/mini-channel-based cooling is considered a promising thermal management technology for electronic devices with high heat flux [11,12].

Generally, microchannel denotes that the hydrodynamic diameter should be 1–100 μm, and the minichannel should be 100–1000 μm [13], respectively. The micro/mini-channel-based thermal management technology has been widely investigated numerically [14,15], experimentally [16], or analytically [17]. Liu and Yu [18] numerically investigated the performance of micro/mini-channel-based heat sink (whose channel dimension is 40 mm × 2.65 mm × 1 mm) and found that the micro/mini-channel-based heat sink can remove a heat flux of 8 W/cm^2 at a pressure loss of 2 kPa. Moreover, the heat transfer capability of the micro/mini-channel-based heat sink can be further enhanced through studying the influencing factors such as substrate material [19] and geometry parameters [20,21]. Tuckerman and Pease [8] experimentally investigated the effect of geometry parameters on the performance of the micro/mini-channel-based heat sink and demonstrated that heat transfer capacity of the micro/mini-channel-based heat sink can be improved by a large aspect-ratio channel. With a channel dimension of 0.05 mm × 0.30 mm × 10 mm, the heat sink can dissipate a maximum heat flux of 790 W/cm^2 but induces a pressure loss of 214 kPa, which means that the demand for pumping capacity is higher. Except for the influencing factors mentioned above, the heat dissipation

Received Nov. 7, 2021; accepted Jan. 7, 2022; online Apr. 25, 2022

Chuanke LIU, Zhizhu HE (✉)
Department of Vehicle Engineering, College of Engineering, China Agricultural University, Beijing 100083, China
E-mail: zzhe@cau.edu.cn

performance of the micro/mini-channel-based heat sink is also restricted by the inherent thermophysical properties of the traditional coolants [22]. Recently, with its non-toxicity, the room-temperature gallium-based liquid metal (LM) is considered as an ultra-high potential extreme thermal management coolant, mainly due to its superior thermal conductivity, high boiling point, and low viscosity [23,24]. In addition, LM can be made into magnetocaloric ferrofluids which can make future fluidic magnetocaloric devices possible [25]. Except for the powerful heat transfer and extraction performance, LM can also be driven by the advanced electromagnetic pumping technology, mainly because of its high electrical conductivity, bringing huge opportunities in advanced thermal management [26].

Electromagnetic pump (EMP) can effectively drive LM without moving parts and any noise, which can outperform traditional pumps (such as peristaltic and mechanical pumps). Generally, EMPs can be classified into direct-current-based electromagnetic pumps (DC-EMPs), alternating-current-based induction electromagnetic pumps (AC-EMPs), and electromagnetic induction pumps with rotating permanent magnets (PM-EMPs), respectively. In a typical DC-EMP, the electromagnetic force was produced by the interaction between the magnetic field and perpendicular direct current, which could drive the LM flow [27] due to Ampere force. Recently, many studies have been conducted focusing on the heat extraction capability of thermal management systems using DC-EMP as the driving source and the LM as the cooling medium, by numerical [28] and experimental approaches [29]. Zhang et al. [30] developed a compact DC-EMP to obtain the driven pressure head of 100 kPa, which is applied to build the LM-based minichannel cooling system. The results show that a super-high heat flux of 300 W/cm^2 could be removed while keeping the heat sink bottom temperature at 75°C. However, the DC-EMP has inevitable disadvantages, such as the current diffuse effect and the electrochemical reaction between liquid metal with electrodes under the condition of high current, which are very unfavorable to its pumping potential. Additionally, the DC-EMP requires a DC power source with a large volume and a high power dissipation, which makes it difficult to perform efficient thermal management for high heat power devices in a limited space [31,32].

Compared with DC-EMP, the PM-EMP is a non-contact driving device with a high-performance driving capacity. The traveling magnetic field was generated by rotating permanent magnets, which produces an induction current within the LM. The electromagnetic force was generated by the interaction between the induced current and the traveling magnetic field, which can provide a powerful pumping force for the LM flow [33]. Wang and Kolesnikov [34] numerically investigated the electromagnetic and flow fields in PM-EMP, which can be used for its performance optimization. Koroteeva et al. [35] investigated the pumping capacity of PM-EMP based on Pb-Li cooling medium and found that the PM-EMP could provide a driving pressure head of 400 kPa and a flow rate of 9 kg/s. Bucenieks [36] developed a high-performance PM-EMP with a pressure head of 500 kPa and a flow rate of over 10 L/s. Many studies were conducted mainly focusing on the applications in nuclear [37,38] and metallurgical industries [39]. However, the research on PM-EMP as a driving source in the thermal management industry of high-power densities electronic devices is very limited.

The literature reviewed above has indicated that the LM-based micro/mini-channel cooling technology has been applied for thermal management with high-power densities. However, its cooling capacity is significantly limited by the pumping method. To solve these problems, this paper developed a minichannel heat dissipation technology based on PM-EMP with a high-pressure head and a large flow rate for thermal management with high heat flux. In addition, the heat transfer and pumping performance of LM-based minichannel heat sink is investigated in detail. First, the PM-EMP and minichannel heat sink were designed and manufactured. Then, the minichannel thermal management system based on the LM was established and experimentally tested at different rotating speeds and heating power. Finally, the heat transfer characteristic of the LM-based minichannel heat sink was theoretically analyzed, and the heat transfer and pumping capacity of the LM-based minichannel thermal management system were experimentally discussed.

2 Experiments and methods

2.1 Coolant of LM preparation

In this paper, $Ga_{68}In_{20}Sn_{12}$ was chosen as the working medium of the thermal management system. The thermophysical properties of $Ga_{68}In_{20}Sn_{12}$ and water are listed in Table 1. The room-temperature LM $Ga_{68}In_{20}Sn_{12}$ was made by the weight of a mixture of 68% gallium, 20% indium, and 12% tin, which was heated and stirred to make it evenly mixed at 200°C.

Table 1 Thermophysical properties of $Ga_{68}In_{20}Sn_{12}$ and water [30,40,41]

Coolant	$\mu/(10^{-3}\text{kg}\cdot(\text{m}\cdot\text{s})^{-1})$	$\rho/(\text{kg}\cdot\text{m}^{-3})$	$c_p/(\text{J}\cdot(\text{kg}\cdot\text{K})^{-1})$	$k/(\text{W}\cdot(\text{m}\cdot\text{K})^{-1})$	Pr
$Ga_{68}In_{20}Sn_{12}$	2.22	6363	366	23.7	0.03
Water	1.003	997	4179	0.606	5.83

2.2 Electromagnetic pump design and fabrication

The PM-EMP was designed based on Ref. [38]. To further improve the reliability and performance of the PM-EMP, two special structures, i.e., the integrated pump body and the iron yoke were designed. Figure 1 shows the new structure of the PM-EMP, which mainly consists of a rotor (a rotating inner iron yoke with permanent magnets, which is mounted on a rotation shaft), a stator (a C-shaped pump duct with rectangular cross-section carrying LM as coolant), and a driving mechanism (a three-phase asynchronous AC motor that drives the rotor to produce rotational motion). The outer radius R of the rotor is 90 mm. The magnet ($Nd_2Fe_{14}B$) size is 75 mm × 25.4 mm × 12 mm with a 1.45 Tesla of the remnant flux density. Eight permanent magnets are mounted at equal intervals (β = 22.5°) on the outer circumference of the inner iron yoke and magnetized alternately along with the radial directions. The inner iron yoke (type 50W470) has a thickness of about 22 mm. The rotor is dragged by a 1.5 kW three-phase asynchronous AC motor to achieve regulatable rotational speeds, which means that a traveling magnetic field is generated. The inner radius R_0 of the stator is 91.5 mm. The C-shaped pump duct (α = 30°) with a 2.5 mm wall thickness and 70 mm × 3.5 mm cross-section is fabricated using non-magnetic stainless steel (304) materials and filled with LM. The integrated pump body structure is formed by welding the pump duct to an understructure, making the PM-EMP more stable during operation. An outer iron yoke (type 50W470) of 10 mm thick was supported by the two side plates to protect the pump duct from excessive pressure, which can provide a low-reluctance magnetic induction line path. Figure 1(c) presents the working principle of the designed PM-EMP. The traveling magnetic field is produced by a rotating inner iron yoke with permanent magnets. The magnetic field passes into the conductive LM filled inside the pump

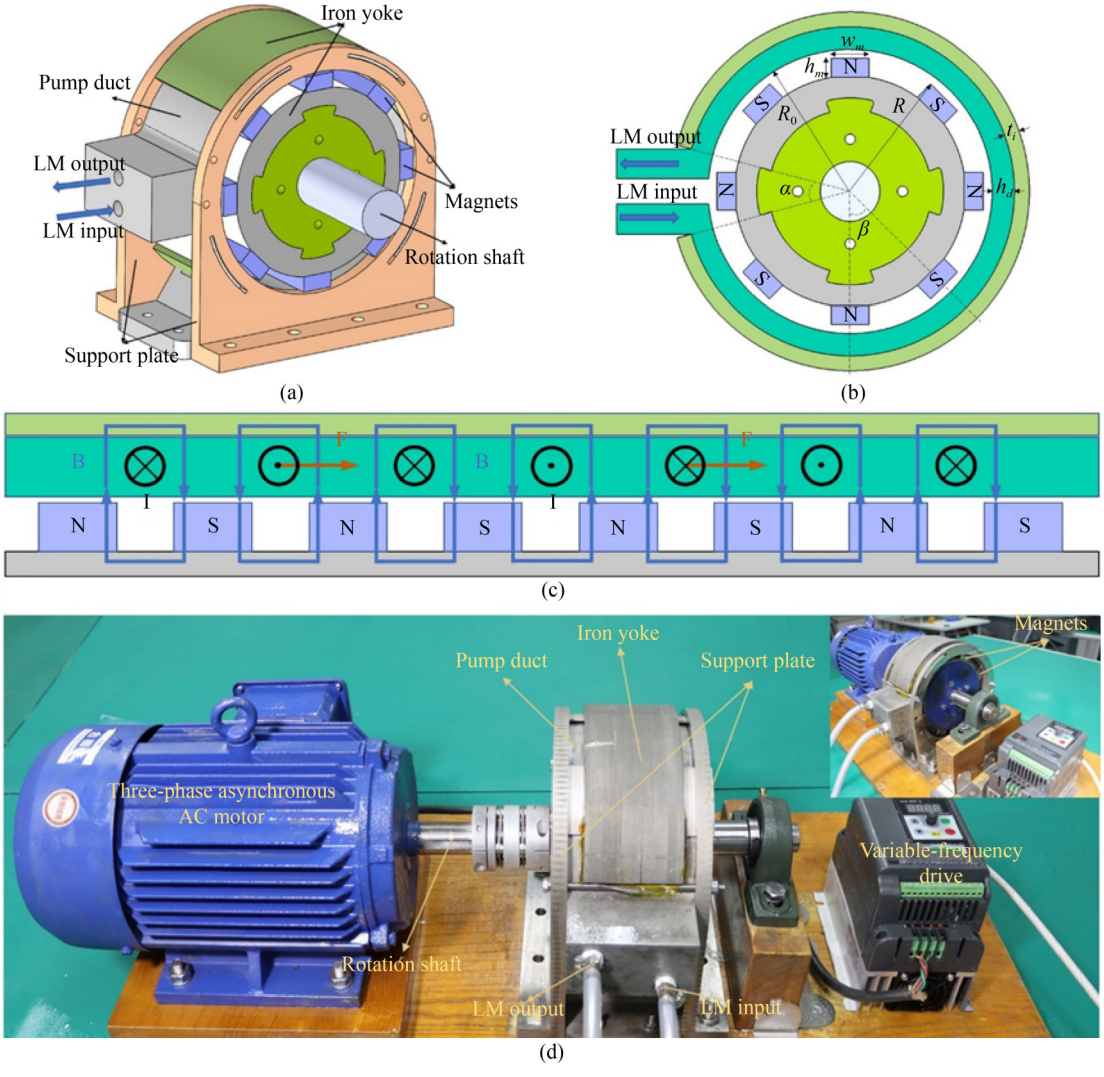

Fig. 1 Illustration of the PM-EMP.
(a) Three-dimensional diagram; (b) diagram of cross-section; (c) working principle; (d) test prototype.

duct, which generates an induction current. The electromagnetic force is produced by the interaction between the traveling magnetic field and the induction current, driving the LM to flow.

2.3 Heat sink design, fabrication, and model

2.3.1 Heat sink design and fabrication

The structure of the heat sink was designed with reference to Ref. [30]. Figure 2 depicts the schematic and detailed dimension of the heat sink, which has a size of 70 mm × 48.5 mm × 10 mm. The channel size is 34 mm × 5 mm × 0.5 mm with a spacing of 0.5 mm and the number of 35, respectively. The channel is fabricated on the base plate (type copper) with a thickness of 2 mm by the milling machine, which is assembled with the cover plate (type copper) by bolts and sealed by polytetrafluoroethylene gaskets. A heat source is formed by inserting seven heating rods into the copper block. The effective heat transfer contact surface area is 2.2 cm × 2.2 cm between the heat sink and the heat source.

2.3.2 Thermal resistance model

The heat transfer performance of a heat sink is usually estimated by thermal resistance, which could be evaluated by many analytical approaches, such as fin analysis, fin-fluid coupled, and porous medium approach. Liu and Garimella [42] suggested using the one-dimension thermal resistance model because of its simplicity and accuracy. The definition of the total thermal resistance R_{total} in the model is

$$R_{\text{total}} = \frac{T_{\text{b}} - T_{\text{hi}}}{Q}, \tag{1}$$

where T_{hi} and T_{b} are the inlet and bottom temperature of the heat sink, and Q is the heat power generated by the heat source, which can be calculated as

$$Q = A \times q, \tag{2}$$

where A is the effective heat transfer contact surface area and q is the heat flux.

The R_{total} can be separated into $R_{\text{conduction}}$ (conduction thermal resistance), R_{capacity} (heat capacity thermal resistance), and $R_{\text{convection}}$ (convection thermal resistance),

$$R_{\text{total}} = R_{\text{conduction}} + R_{\text{capacity}} + R_{\text{convection}}, \tag{3}$$

which can be expressed as

$$R_{\text{conduction}} = \frac{t_{\text{b}}}{k_{\text{b}} W L}, \tag{4}$$

$$R_{\text{convection}} = \frac{1}{N h l_{\text{c}} (w_{\text{c}} + 2\eta_{\text{f}} \text{h}_{\text{c}})}, \tag{5}$$

$$R_{\text{capacity}} = \frac{1}{\dot{m}\, c_{\text{p}}} = \frac{1}{N \rho U_i h_{\text{c}} w_{\text{c}} c_{\text{P}}}, \tag{6}$$

where U_i, ρ, c_{p}, and m are the average velocity, density, heat capacity, and mass flow rate of the coolant; L, W, t_{b}, and k_{b} are the length, width, thickness, and thermal conductivity of the base plate of heat sink; l_{c}, h_{c}, w_{c}, and N are the length, height, width, and number of the the minichannel; $\eta_{\text{f}} = \tan(hmh_{\text{c}})/(mh_{\text{c}})$ ($m = (2h/(k_{\text{b}} w_{\text{w}})^{1/2}$) is the efficiency of the channel fin; h is the heat transfer coefficient, which can be calculated by

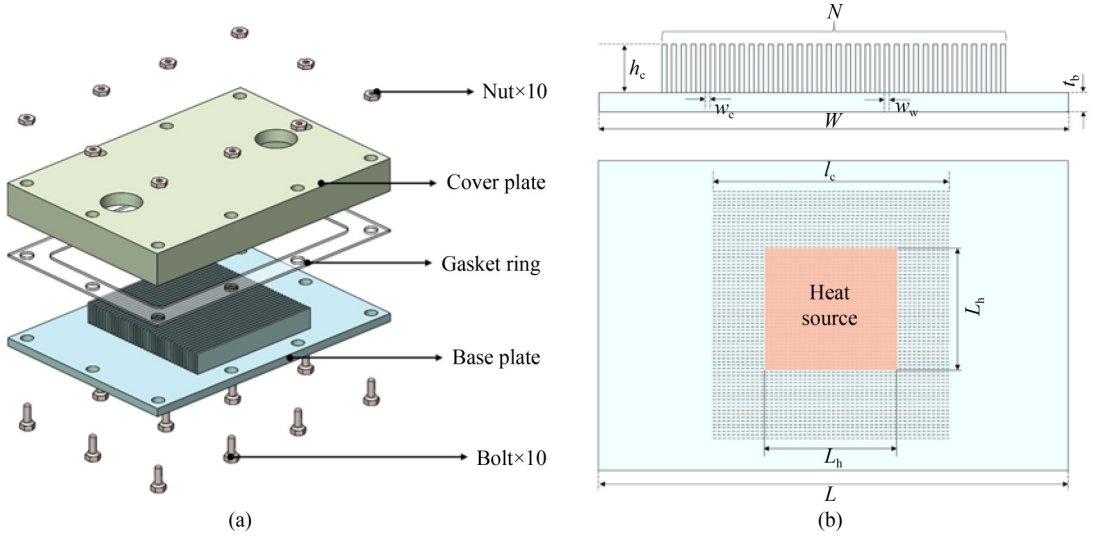

Fig. 2 Illustration of the minichannel heat sink.
(a) Three-dimensional diagram; (b) two-dimensional diagram.

$$h = \frac{kNu}{D_h}, \tag{7}$$

where k is the thermal conductivity of coolant, $D_h = 2w_c h_c/(w_c + h_c)$ is the hydraulic diameter of the heat sink, and Nu is the Nusselt number. The Nusselt number for fully developed laminar flow reads as [20]

$$Nu_{fd} = 8.235 - 16.817a + 25.407a^2 - 20.394a^3 + 8.711a^4 - 1.533a^5. \tag{8}$$

The Nusselt number for thermally developing laminar flow is [43]

$$Nu = 1.87Pr^{-0.036}a^{-0.056}(x^*)^{-0.3}, 0.005 < x^* < 0.013,$$
$$Nu = 3.35Pr^{-0.038}a^{-0.12}(x^*)^{-0.13}, 0.013 \leqslant x^* < 0.1, \tag{9}$$

$$x^* = \frac{x}{D_h RePr}, \ 0 < x \leqslant L_c, \tag{10}$$

where $a = w_c/h_c$ is the aspect ratio of the minichannel, x^* is the distance for the thermal entrance region, Pr and Re are the Prandtl and Reynolds numbers, respectively.

2.4 Experimental setup

To experimentally study the heat removal capacity of the minichannel heat sink based on the LM, a thermal management system was built. The experimental setup was presented in Fig. 3, including a minichannel heat sink, a heat source, a PM-EMP, a radiator, an electromagnetic flowmeter, a pressure sensor, a reservoir, a valve, and a data acquisition system, respectively. During the entire heat transfer process, heat power (whose value was adjusted by a voltage regulator) was first produced by the heat source wrapped with the adiabatic sponge. Then, the heat was absorbed by the flowing LM within the heat sink. Finally, it was transferred into the radiator, and dissipated into the atmosphere through convective heat transfer. In addition, the LM was continuously pumped by the PM-EMP. The flow rate and pressure loss of the heat sink were obtained by an electromagnetic flowmeter (with a range from 0 to 1.4 m^3/h and an accuracy of ±0.5%) and two pressure sensors (with a range from 0 to 300 kPa and an accuracy of ±0.10%), respectively. The temperature of the heat source was monitored by two K-type thermocouples (with a range from –20 to 200 °C and an accuracy of ±0.50 °C). The inlet/outlet temperatures of the heat sink and radiator were measured by four K-type thermocouples. All the temperature signs were gathered by the Agilent 34970A data acquisition.

The uncertainty analysis [44] for the Reynolds number and thermal resistance was conducted by using Eqs. (11) and (12),

$$\frac{\delta Re}{Re} = \frac{1}{Re}\frac{\rho D_h}{\mu}\delta U_i, \tag{11}$$

$$\frac{\delta R}{R} = \frac{1}{R}\sqrt{\left(\frac{\partial R}{\partial Q}\delta Q\right)^2 + \left(\frac{\partial R}{\partial T}\delta T\right)^2}. \tag{12}$$

The maximum relative errors of Re and R were calculated as 0.50% and 4.04%, respectively. The uncertainty of main parameters is listed in Table 2.

Table 2 Uncertainty of main parameters

Parameters	G/%	P/%	T/°C	Q/%	Re/%	R/%
Maximum uncertainty	±0.50	±0.10	±0.50	±1.41	±0.50	±4.04

3 Results and discussion

3.1 Pumping performance of the PM-EMP

The change of pressure head versus flow rate under different rotational speeds (from 50 to 400 r/min) is presented in Fig. 4. It is observed that the maximum pressure head of the PM-EMP is 160 kPa at 400 r/min, and the maximum flow rate is 3.24 L/min at 400 r/min, indicating that the PM-EMP is sufficiently capable of driving the LM to flow through the minichannel heat sink. The pressure head drops steadily with the flow rate at different rotational speeds, making the PM-EMP operation more stable, which means that the PM-EMP is superior to conventional pumps to drive the LM. For instance, for n = 300 r/min, with the flow rate increasing from 0 to 2.74 L/min, the pressure head smoothly decreased from 130 to 27 kPa. It is also found that the driven pressure head can be significantly increased by increasing the rotational speed. For example, when n = 50 r/min, ΔP = 20 kPa, but when n = 300 r/min, ΔP = 130 kPa. The reason for this is that the electromagnetic force is proportional to the induced current (which is increased as the rotational speed increases). Moreover, the results indicate that as the rotational speed increases, the flow rate also increases. For example, the maximum flow rate could increase from 0.88 to 2.74 L/min (corresponding velocity of the LM from 0.06 to 0.19 m/s in the pump duct) with an increase in rotational speed from 50 to 300 r/min. It is noteworthy that the 220 V AC supply for PM-EMP is more easily obtained compared with the DC supply with a high output current for DC-EMP.

3.2 Cooling performance demonstration of the thermal management system

To guarantee the accuracy and reliability of the experimental data, it is very indispensable to conduct a thermal response analysis of the cooling system. When heat flux increases from 120 (581 W) to 138 W/cm^2 (669 W) at n = 100 r/min, the transient temperature rise curve of the thermal management system is described in Fig. 5.

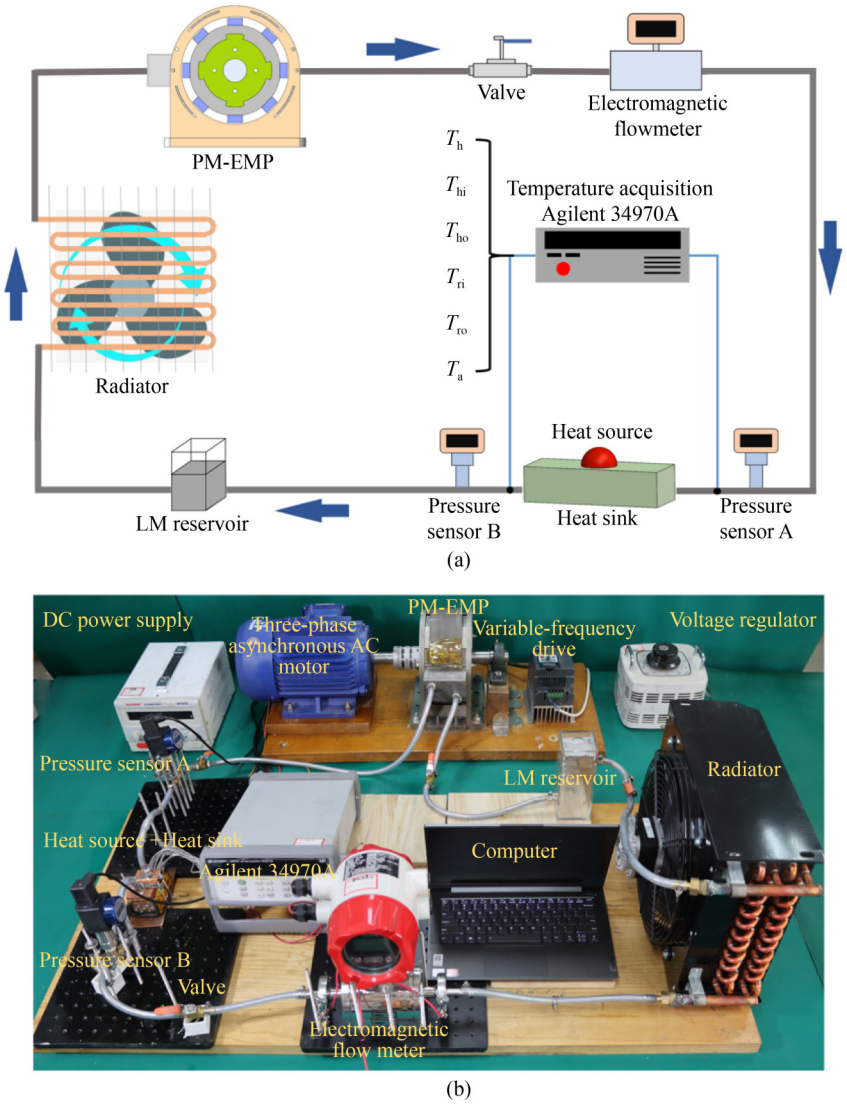

Fig. 3 Description of the test loop.
(a) Schematic illustration; (b) experiment platform.

It can be seen that the thermal response time of the system is about 280 s. It is also found that the temperature difference of LM ($T_{ho} - T_{hi}$) has an increase of 2.6 °C (from 13.4 to 16.0 °C), but T_h varies from 57.6 to 64.0 °C, which means that the heat from the heat source is not efficiently absorbed by the LM. The main reason for this is that, except for the convection thermal, resistance, the effect of thermal contact resistance (between the heat sink and the heat source) cannot be neglected on the cooling performance in case of a high heat flux. On account of its excellent thermal conductivity, LM has been investigated not only as coolants but also as thermal interface materials in this paper.

The heat transfer performance of the LM-based minichannel thermal management system at a rotating speed of n = 200 r/min is analyzed comparably at different heat fluxes when the LM thermal grease and the

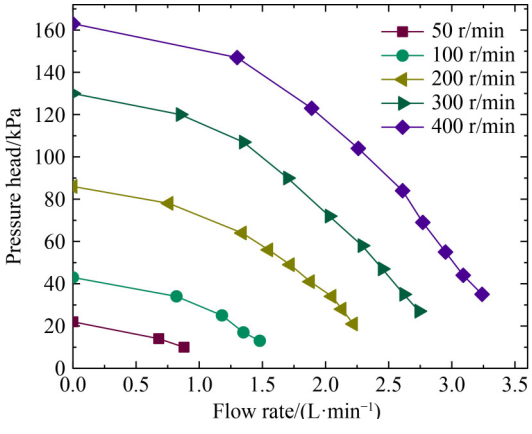

Fig. 4 Pressure head versus flow rate at different rotational speeds.

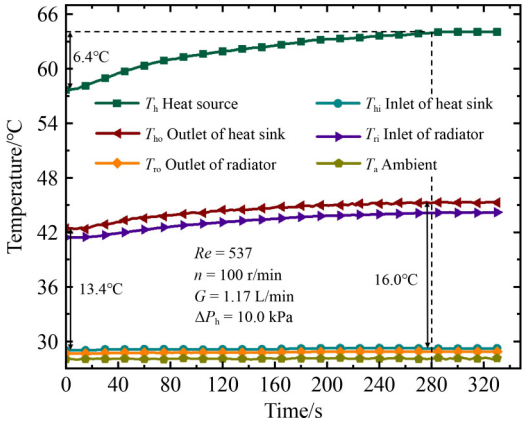

Fig. 5 Transient temperature rise of the cooling system when heat flux increases from 120 (581 W) to 138 W/cm^2 (669 W) at n = 100 r/min.

traditional thermally conductive silicone grease were used as thermal interface materials, respectively, as presented in Fig. 6. The Reynolds number of LM is calculated as 790 in the minichannel heat sink. The pressure loss of the minichannel heat sink is measured as 19.0 kPa and the flow rate of the LM-based cooling system is obtained at 1.72 L/min. It can be seen that with the heat flux increasing, T_h, T_{ho}, and T_{ri} rise linearly, but T_{hi} and T_{ro} almost remain unchanged, which means that the heat from the heat source is effectively released to the ambient by the heat sink and radiator with a powerful heat dissipation ability. In addition, by comparing the results of Fig. 6(a) (using LM thermal grease) and Fig. 6(b) (using thermally conductive silicone grease), it can be easily concluded that the cooling capacity of the thermal management system can be further enhanced by using LM thermal grease as thermal interface material. For example, T_h is 61.0°C (from Fig. 6(a)) compared with 65.8°C (from Fig. 6(b)) when q equals 150 W/cm^2, which is decreased by 4.8°C when using LM thermal grease. The reason lies in the fact that compared with the thermally conductive silicone grease, the thermal contact resistance of the cooling system can be efficiently reduced by using the LM thermal grease with a high thermal conductivity.

When the LM thermal grease and the traditional thermally conductive silicone grease were used as thermal interface materials respectively, the variation of ΔT_h ($T_h - T_a$) with rotating speed n (from 100 to 300 r/min) is also tested at different heat fluxes, as presented in Fig. 7. Re varied between 537 (100 r/min) and 974 (300 r/min). This results indicate that with q increasing, ΔT_h linearly increased. For example, with q increasing from 79 to 203 W/cm^2, ΔT_h linearly increased from 18.4°C to 53.6°C when n equals 100 r/min, as shown in Fig. 7(a) (using the LM thermal grease). It is also found that the slope of ΔT_h and q gradually decreased with n increasing, which means that the total thermal resistance decreases as n increases. In addition, a comparison of Figs. 7(a) and 7(b) further proves that the heat transfer enhancement is obtained by using the LM thermal grease as the thermal interface material. For example, when keeping ΔT_h below 50°C, compared with a heat of 208 W/cm^2 (from Fig. 7(b)), the cooling system can dissipate up to a heat of 242 W/cm^2 (from Fig. 7(a)), which means that q is increased by 32 W/cm^2 when using the LM thermal grease.

The heat transfer performance of the minichannel heat sink tested at different rotating speeds (from 100 to 300 r/min) at a heat flux of 165 W/cm^2 is manifested in Fig. 8. It can be found that with the rotating speed of n increasing, ΔT_h first decreases rapidly, and then declines slowly. For example, when the silicone grease is used as the thermal interface material, ΔT_h has a decrease of 8.0 °C (from 50.1 to 42.1 °C) with increasing n from 100 to 200 r/min, but ΔT_h just decreases by 1.7 °C (from 42.1 to 40.4 °C) with n increasing from 200 to 300 r/min. The test results indicate that the cooling performance of the minichannel heat sink cannot be consistently enhanced by

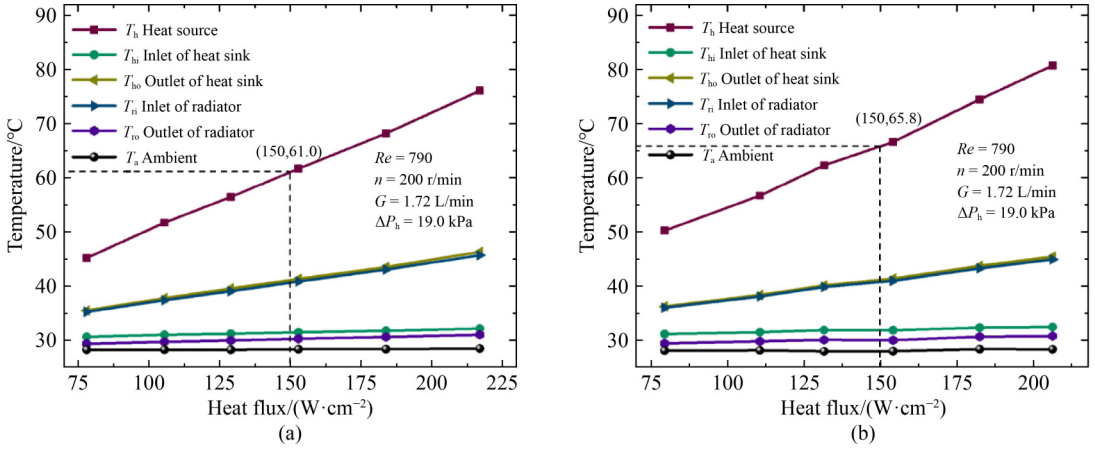

Fig. 6 Temperature of the thermal management system at a rotating speed of 200 r/min at different heat fluxes. (a) Using the LM thermal grease; (b) using the thermally conductive silicone grease.

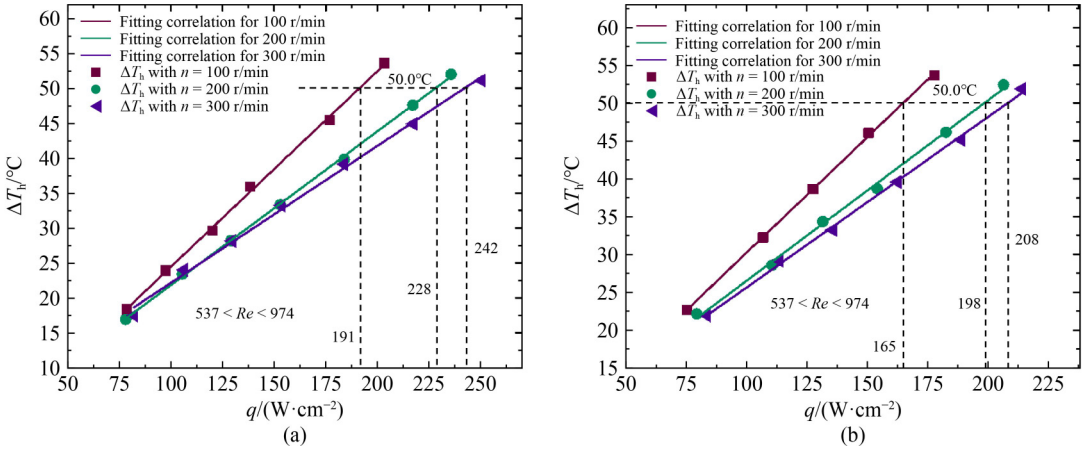

Fig. 7 ΔT_h versus q (100 r/min, 200 r/min, and 300 r/min)
(a) Using the LM thermal grease; (b) using the thermally conductive silicone grease.

increasing the rotating speed of n. The reasons for the above phenomenon will be analyzed in Section 3.3. Moreover, compared with using the thermally conductive silicone grease, ΔT_h is obviously lower when using the LM thermal grease. For example, at n = 100 r/min and q = 165 W/cm^2, ΔT_h decreases to 7.4°C when using the LM thermal grease.

Figure 9 shows the fluid flow characteristic of the LM in the minichannel heat sink at different rotating speeds (from 100 to 300 r/min) at a heat flux of 165 W/cm^2. It can be seen that ΔP_h and G increase as n increases. For instance, ΔP_h and G increase from 10 kPa and 1.17 L/min at n = 100 r/min to 29 kPa and 2.12 L/min at n = 300 r/min, which means that a greater pumping capacity is easily achieved by adopting a higher rotating speed, thereby improving the LM heat transfer performance.

3.3 Thermal resistance analysis of the minichannel heat sink

The thermal resistance of the minichannel heat sink can also be described by the ratio of temperature difference (obtained by experiment) to thermal power. The total thermal resistance R'_{total} can be calculated by

$$R'_{total} = \frac{T_h - T_{hi}}{Q}, \tag{13}$$

where T_h is the temperature of the heat source. Compared with R_{total} (Eq. (1)), because R'_{total} is defined by T_h, the thermal contact resistance $R_{contact}$ (between the heat sink with the heat source) should also be considered in R'_{total}. In another word, $R_{contact}$ was divided into the heat capacity thermal resistance $R'_{capacity}$, the conduction thermal resistance R'_{total}, the convection thermal resistance $R'_{convection}$, and the thermal contact resistance $R_{contact}$, i.e.,

$$R'_{total} = R'_{capacity} + R'_{conduction} + R'_{convection} + R_{contact}. \tag{14}$$

However, it is difficult to directly obtain $R'_{convection}$ and $R_{contact}$ by experiment. Therefore, R'_{total} was separated into R_{other} and $R'_{capacity}$ in this paper, which is defined as

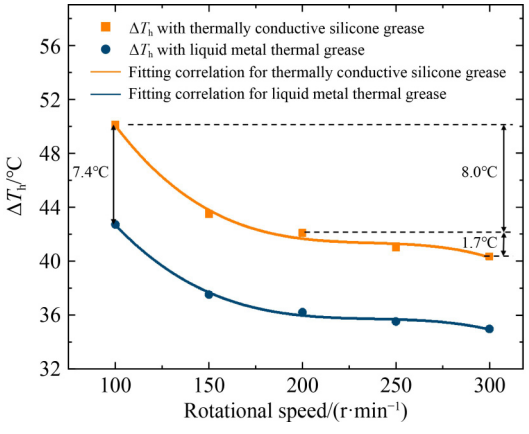

Fig. 8 Heat transfer characteristics of minichannel heat sink at different rotational speeds (from 100 to 300 r/min) at a heat flux of 165 W/cm^2.

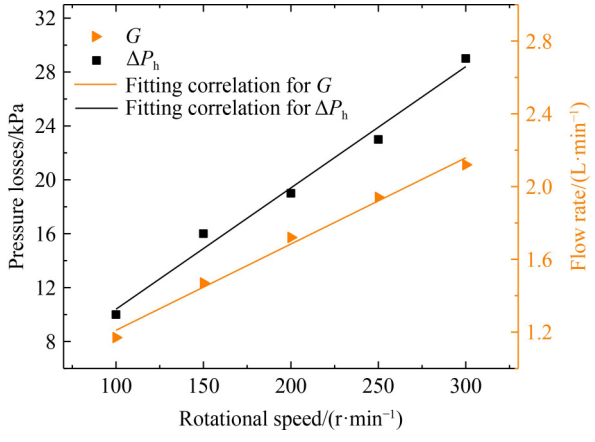

Fig. 9 Fluid flow characteristic of minichannel heat sink at different rotational speeds (from 100 to 300 r/min) at a heat flux of 165 W/cm^2.

$$R_{\text{other}} = R'_{\text{conduction}} + R'_{\text{convection}} + R_{\text{contact}} = \frac{T_{\text{h}} - T_{\text{m}}}{Q}, \quad (15)$$

$$R'_{\text{capacity}} = \frac{T_{\text{m}} - T_{\text{hi}}}{Q}, \quad (16)$$

where T_{m} is the mean value of T_{hi} and T_{ho}.

When the LM thermal grease and traditional thermally conductive silicone grease were used as thermal interface materials respectively, the variation of R'_{capacity} and R_{other} with rotating speed n (100, 200, 300 r/min) is shown in Fig. 10. It is found that R'_{total} gradually decreases as n increases. For example, R'_{total} decreases from 0.05942 at n = 100 r/min to 0.04351 °C/W at n = 300 r/min (using thermally conductive silicone grease). In addition, it is noteworthy that in the case of thermally conductive silicone grease, R'_{total} decreases by 0.01193 °C/W (from 0.05942 to 0.04749 °C/W) with n increasing from 100 to 200 r/min, but R'_{total} just decreases by 0.00398°C/W (from 0.04749 to 0.04351°C/W) with n increasing from 200 to 300 r/min, which explains the variation of ΔT_{h} (Fig. 8). Moreover, at the same n (which means that U_{i} is constant), $R'_{\text{conduction}}$ and $R'_{\text{convection}}$ are almost constant for using different thermal interface materials (LM thermal grease or thermally conductive silicone grease), which means that R_{contact} can be analyzed by R_{other} according to Eq. (15). Therefore, compared with using the thermally conductive silicone grease, R_{contact} decreases by about 0.00777 °C/W when using the LM thermal grease.

The comparative analysis of the mathematical model and the experimental results (using LM thermal grease) is exhibited in Table 3. It can be found that compared with two sets of results, the relative deviation ε of the total thermal resistance is calculated as 24.18%, 25.06%, and 27.36% (for n from 100 to 300 r/min), respectively. The reason lies in the fact that it is difficult to accurately define R_{contact} by using specific analytical formulas. Therefore, the effect of R_{contact} is not considered in the mathematical model (according to Eq. (3)). In addition, the fundamental requisite for establishing the mathematical model is that the flow is in fully developed conditions (thermal and hydrodynamic). Moreover, according to Eqs. (3) – (10), to further demonstrate the advantages of the LM coolant (compared with water coolant), the difference between $R_{\text{total–LM}}$ (using LM coolant) and $R_{\text{total–Water}}$ (using water coolant) is summarized in Table 4. It can be found that the ratio a of the total thermal resistance is calculated as 1.264, 1.437, and 1.526 (n increases from 100 to 300 r/min), which means that an efficient heat dissipation of the cooling system can be obtained by using the LM coolant.

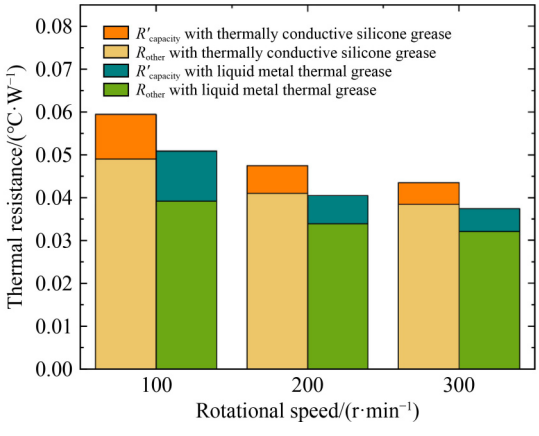

Fig. 10 R'_{capacity} and R_{other} versus rotational speed n (100, 200, 300 r/min).

Table 3 Deviation between R'_{total} and R_{total} at different rotating speeds

n/(r·min^{-1})	R'_{total}/(10^{-2} °C·W^{-1})	R_{total}/(10^{-2} °C·W^{-1})	ε/%
100	5.091	3.860	24.18
200	4.050	3.035	25.06
300	3.735	2.713	27.36

Table 4 Difference between $R_{\text{total–LM}}$ and $R_{\text{total–Water}}$ at different rotating speeds

n/(r·min^{-1})	$R_{\text{total–LM}}$/(10^{-2} °C·W^{-1})	$R_{\text{total–Water}}$/(10^{-2} °C·W^{-1})	a ($R_{\text{total–Water}}$/$R_{\text{total–LM}}$)
100	3.860	4.880	1.264
200	3.035	4.360	1.437
300	2.713	4.141	1.526

4 Conclusions

A minichannel heat dissipation technology is developed based on high-performance electromagnetic induction pump for high heat-flux thermal management. The thermal and hydrodynamic characteristics of the liquid metal-based minichannel cooling system are experimentally investigated in detail. The main results can be summarized as follows.

A high-performance electromagnetic induction pump is developed by the integrated design of the pump body and iron yoke with a supporting structure. The driving performance of the electromagnetic induction pump is demonstrated by the principle experiment. The maximum pressure head is achieved and the flow rate of the electromagnetic induction pump is 160 kPa at 400 r/min, and 3.24 L/min at 400 r/min, meaning that the electromagnetic induction pump is sufficiently capable of driving the liquid metal in the minichannel heat sink. It is also found that increasing rotational speed could significantly enhance the performance of the electromagnetic induction pump. Moreover, it is noteworthy that the pressure head smoothly drops with the flow rate, which makes the electromagnetic induction pump operate more stably.

A liquid metal-based minichannel thermal management system is established and experimentally tested to investigate the thermal and hydrodynamic characteristics.

The results indicate that when keeping the temperature rise of the heat source below 50 °C, the cooling system can remove a heat flux of 242 W/cm^2. It is noteworthy that the heat transfer capability of the liquid metal-based minichannel heat sink could be considerably enhanced by increasing the rotating speed n (especially for at a variation of n from 100 to 200 r/min).

Thermal contact resistance is an important influencing factor for the heat dissipation capacity of high heat-flux thermal management. Compared with the traditional thermally conductive silicone grease, the LM thermal grease with an excellent thermal conductivity can more efficiently reduce the thermal contact resistance. For instance, the thermal contact resistance decreases by about 7.77×10^{-3} °C/W, which would significantly improve the temperature rise of the heat source (ΔT_h decreases by 7.4 °C at n = 100 r/min and q = 165 W/cm^2).

In summary, the liquid metal-based minichannel cooling technology driven by the high-performance electromagnetic induction pump is a promising candidate for the thermal management of electric devices with a large heat power and a high heat flux.

Acknowledgments This work was supported by the National Natural Science Foundation of China (No. 52076213) and the 2115 Talent Development Program of China Agricultural University.

Notations

a	Minichannel aspect ratio
D_h	Heat sink hydraulic diameter/mm
G	Flow rate/(L·min^{-1})
h_c	Minichannel height/mm
h_d	Pump duct height/mm
h_m	Magnet height/mm
L	Heat sink total length/mm
l_c	Minichannel length/mm
N	Minichannel number
n	Rotating speed of PM-EMP/(r·min^{-1})
P	Pressure/Pa
ΔP	Pressure difference of PM-EMP/Pa
ΔP_h	Pressure loss of heat sink/Pa
R	Outer radius of rotor of PM-EMP/mm
R_0	Inner radius of stator of PM-EMP/mm
T	Temperature/°C
T_a	Ambient temperature/°C
T_b	Heat sink bottom temperature/°C
T_h	Heat source temperature/°C
T_{hi}	Heat sink inlet temperature/°C
T_{ho}	Heat sink outlet temperature/°C
T_{ri}	Radiator inlet temperature/°C
T_{ro}	Radiator outlet temperature/°C
ΔT_h	Heat source temperature rise/°C
t_i	Thickness of iron yoke of PM-EMP/mm
W	Heat sink total width/mm
w_c	Minichannel width/mm
w_m	Magnet width/mm
w_w	Minichannel wall width/mm

References

1. Yang X H, Liu J. Advances in liquid metal science and technology in chip cooling and thermal management. Advances in Heat Transfer, 2018, 50: 187–300
2. Hamidnia M, Luo Y, Wang X D. Application of micro/nano technology for thermal management of high power LED packaging–a review. Applied Thermal Engineering, 2018, 145: 637–651
3. Habibi Khalaj A, Halgamuge S K A Review on efficient thermal management of air-and liquid-cooled data centers: from chip to the cooling system. Applied Energy, 2017, 205: 1165–1188
4. Qian Z, Li Y, Rao Z. Thermal performance of lithium-ion battery thermal management system by using mini-channel cooling. Energy Conversion and Management, 2016, 126: 622–631
5. Lee J, Ki S, Seo D, et al. Liquid cooling module incorporating a metal foam and fin hybrid structure for high power insulated gate bipolar transistors (IGBTs). Applied Thermal Engineering, 2020, 173: 115230
6. Liu D, Zhao F Y, Yang H X, et al. Thermoelectric mini cooler coupled with micro thermosiphon for CPU cooling system. Energy, 2015, 83: 29–36
7. Yeh L T. Review of heat transfer technologies in electronic equipment. Journal of Electronic Packaging, 1995, 117(4): 333–339
8. Tuckerman D B, Pease R F W. High-performance heat sinking for VLSI. IEEE Electron Device Letters, 1981, 2(5): 126–129
9. Feng Z, Li P. Fast thermal analysis on GPU for 3D ICs with integrated microchannel cooling. IEEE Transactions on Very Large Scale Integration Systems, 2012, 21(8): 1526–1539
10. Chein R, Chuang J. Experimental microchannel heat sink performance studies using nanofluids. International Journal of Thermal Sciences, 2007, 46(1): 57–66
11. Dixit T, Ghosh I. Review of micro-and mini-channel heat sinks and heat exchangers for single phase fluids. Renewable & Sustainable Energy Reviews, 2015, 41: 1298–1311
12. Mahalingam M. Thermal management in semiconductor device packaging. Proceedings of the IEEE, 1985, 73(9): 1396–1404
13. Mehendale S S, Jacobi A M, Shah R K. Fluid flow and heat transfer at micro-and meso-scales with application to heat exchanger design. Applied Mechanics Reviews, 2000, 53(7): 175–193
14. Muhammad A, Selvakumar D, Wu J. Numerical investigation of laminar flow and heat transfer in a liquid metal cooled mini-channel heat sink. International Journal of Heat and Mass Transfer, 2020, 150: 119265
15. Xie X L, Liu Z J, He Y L, et al. Numerical study of laminar heat

transfer and pressure drop characteristics in a water-cooled minichannel heat sink. Applied Thermal Engineering, 2009, 29(1): 64–74
16. Sohel M R, Khaleduzzaman S S, Saidur R, et al. An experimental investigation of heat transfer enhancement of a minichannel heat sink using Al_2O_3-H_2O nanofluid. International Journal of Heat and Mass Transfer, 2014, 74: 164–172
17. Ijam A, Saidur R, Ganesan P. Cooling of minichannel heat sink using nanofluids. International Communications in Heat and Mass Transfer, 2012, 39(8): 1188–1194
18. Liu X, Yu J. Numerical study on performances of mini-channel heat sinks with non-uniform inlets. Applied Thermal Engineering, 2016, 93: 856–864
19. Hung T C, Yan W M, Li W P. Analysis of heat transfer characteristics of double-layered microchannel heat sink. International Journal of Heat and Mass Transfer, 2012, 55(11−12): 3090–3099
20. Yang X H, Tan S C, Ding Y J, et al. Flow and thermal modeling and optimization of micro/mini-channel heat sink. Applied Thermal Engineering, 2017, 117: 289–296
21. Wang H, Chen Z, Gao J. Influence of geometric parameters on flow and heat transfer performance of micro-channel heat sinks. Applied Thermal Engineering, 2016, 107: 870–879
22. Lee J, Mudawar I. Assessment of the effectiveness of nanofluids for single-phase and two-phase heat transfer in micro-channels. International Journal of Heat and Mass Transfer, 2007, 50(3−4): 452–463
23. Wang Q, Yu Y, Liu J. Preparations, characteristics and applications of the functional liquid metal materials. Advanced Engineering Materials, 2018, 20(5): 1700781
24. Cao L X, Yin T, Jin M X, et al. Flexible circulated-cooling liquid metal coil for induction heating. Applied Thermal Engineering, 2019, 162: 114260
25. de Castro I A, Chrimes A F, Zavabeti A, et al. A gallium-based magnetocaloric liquid metal ferrofluid. Nano Letters, 2017, 17(12): 7831–7838
26. Gu J, She J, Yue Y. Micro/nanoscale thermal characterization based on spectroscopy techniques. ES Energy & Environment, 2020, 9(2): 15–27
27. Zhang X D, Zhou Y X, Liu J. A novel layered stack electromagnetic pump towards circulating metal fluid: design, fabrication and test. Applied Thermal Engineering, 2020, 179: 115610
28. Tawk M, Avenas Y, Kedous-Lebouc A, et al. Numerical and experimental investigations of the thermal management of power electronics with liquid metal mini-channel coolers. IEEE Transactions on Industry Applications, 2013, 49(3): 1421–1429
29. Sun P, Zhang H, Jiang F C, et al. Self-driven liquid metal cooling connector for direct current high power charging to electric vehicle. eTransportation, 2021, 10: 100132
30. Zhang X D, Yang X H, Zhou Y X, et al. Experimental investigation of galinstan based minichannel cooling for high heat flux and large heat power thermal management. Energy Conversion and Management, 2019, 185: 248–258
31. Zhou X, Gao M, Gui L. A liquid-metal based spiral magnetohydrodynamic micropump. Micromachines, 2017, 8(12): 365
32. Wang Y, Zhang P, Tan S, et al. Experimental and numerical analysis on a compact liquid metal blade heat dissipator with twin stage electromagnetic pumps. International Communications in Heat and Mass Transfer, 2019, 104: 15–22
33. Bucenieks I E. Perspectives of using rotating permanent magnets in the design of electromagnetic induction pumps. Magnetohydrodynamics, 2000, 151–156
34. Wang X, Kolesnikov Y. A numerical visualization of physical fields in an electromagnetic pump with rotating permanent magnets. Magnetohydrodynamics, 2014, 50(2): 139–156
35. Koroteeva E, Ščepanskis M, Bucenieks I, et al. Numerical modeling and design of a disk-type rotating permanent magnet induction pump. Fusion Engineering and Design, 2016, 106: 85–92
36. Bucenieks I E. High pressure and high flowrate induction pumps with permanent magnets. Magnetohydrodynamics, 2003, 39(4): 411–418
37. Hvasta M G, Nollet W K, Anderson M H. Designing moving magnet pumps for high-temperature, liquid-metal systems. Nuclear Engineering and Design, 2018, 327: 228–237
38. Mirhoseini S M H, Diaz-Pacheco R R, Volpe F A. Passive and active electromagnetic stabilization of free-surface liquid metal flows. Magnetohydrodynamics, 2017, 53(1): 45–54
39. Bojarevics A, Beinerts T, Gelfgat Y, et al. Permanent magnet centrifugal pump for liquid aluminium stirring. International Journal of Cast Metals Research, 2016, 29(3): 154–157
40. Miner A, Ghoshal U. Cooling of high-power-density microdevices using liquid metal coolants. Applied Physics Letters, 2004, 85(3): 506–508
41. Bergman T L, Incropera F P, DeWitt D P, et al. Fundamentals of Heat and Mass Transfer. New York: John Wiley & Sons, 2011
42. Liu D, Garimella S V. Analysis and optimization of the thermal performance of microchannel heat sinks. International Journal of Numerical Methods for Heat & Fluid Flow, 2005, 15(1): 7–26
43. Harms T M, Kazmierczak M J, Gerner F M. Developing convective heat transfer in deep rectangular microchannels. International Journal of Heat and Fluid Flow, 1999, 20(2): 149–157
44. Holman J P, Gajda W J. Experimental Methods for Engineers. 5th ed. New York: McGraw-Hill, 1989